

# 1 Identification of the hygro-thermo-chemical-mechanical model 2 parameters of concrete through inverse analysis

3 Massimiliano Bocciarelli<sup>1\*</sup>, Gianluca Ranzi<sup>2</sup>

4 <sup>1</sup> Architecture, Built environment and Construction engineering Department, Politecnico di  
5 Milano (Technical University), Italy

6 <sup>2</sup> School of Civil Engineering, The University of Sydney, Australia

7 \* Corresponding Author. E-mail: [massimiliano.bocciarelli@polimi.it](mailto:massimiliano.bocciarelli@polimi.it)

## 8 Abstract

9 A wide range of parameters is required in input when applying hygro-thermo-chemical-  
10 mechanical models to concrete components with the aim of determining the variations over time  
11 of temperature, relative humidity and shrinkage induced deformations. While a sub-set of these  
12 material parameters can be evaluated on the basis of the concrete mix specifications or from  
13 literature data, this paper presents a robust inverse analysis procedure for the identification of  
14 the remaining sub-set of parameters that are characterised by a large variability and, in some  
15 cases, do not have a precise physical meaning and are not amenable to a direct measurement.  
16 The particularity of this paper is to propose different strategies for the characterisation of these  
17 material parameters that account for the presence of different exposure conditions, as these affect  
18 the outcomes and requirements of the parameter identification procedure. After introducing the  
19 adopted hygro-thermo-chemical-mechanical model, representative results of an extensive  
20 sensitivity analysis are presented in the first part of the paper to give insight into most effective  
21 number, location and duration of measurements to be used in input of the inverse analysis. The  
22 inverse analysis procedure is then presented and applied to a number of selected scenarios to  
23 highlight its robustness considering different boundary conditions in terms of external  
24 temperature and relative humidity surrounding the concrete. The ability to characterise these  
25 parameters will support a wider use of these hygro-thermo-chemical-mechanical models,  
26 especially for those applications in which humidity and temperature profiles significantly  
27 influence the structural response, for example when predicting curling in industrial pavements  
28 and non-uniform shrinkage profiles in composite steel-concrete slabs.

## 29 Keywords

30 Concrete; inverse analysis; long-term behaviour; moisture diffusion; sensitivity analysis;  
31 shrinkage.

## 32 **1. Introduction**

33 Concrete structures are significantly influenced by the time-dependent behaviour of the concrete  
34 that affects their serviceability and durability. An inaccurate evaluation of this service response  
35 can lead to undesired excessive deformations and occurrence of cracking. Concrete time effects  
36 are significantly dependent on the moisture transport and heat transfer mechanisms that take  
37 place in the concrete and that control, for example, the hardening process, water release, cement  
38 hydration, and volume changes. Different numerical and experimental studies are available in  
39 the literature that deal with the concrete behaviour, especially considering its early age. Bažant  
40 and Najjar [1] presented a material model capable of describing the nonlinear moisture transport  
41 that takes place in concrete. Several researchers extended this approach in following years, for  
42 example, by incorporating a thermodynamics based approach for the cement hydration [2] or by  
43 establishing a thermo-chemo-mechanical model to account for the aging effect on strength  
44 development and the micro-scale description of the material [3-5]. Other recent contributions  
45 considered the influence of cracking on the permeability [6] or included a sink term into the  
46 diffusive moisture equation to capture the internal water consumption occurring during cement  
47 hydration [7,8]. The use of an enhanced cement hydration model was presented in [9] while the  
48 influence of the meso-structure was investigated in [10-12]. A hygro-thermo-chemical model  
49 that accounted for the effect of cement hydration on both moisture and temperature calculations  
50 was considered in [13,14]. The mechanical coupling is usually based on a linear relationship  
51 between the variations over time of the relative humidity and the consequent free shrinkage  
52 deformations (see, e.g. [13,14,15,16]).

53 The use of these models is particularly relevant in applications where the effect of shrinkage  
54 induced deformations are important, such as curling in industrial pavements [17,18] and  
55 shrinkage gradients in composite floor systems [19-22] (where the presence of different exposure  
56 conditions, due to the presence of subgrade/waterproofing membrane and profiled steel sheeting,  
57 respectively, influence the mechanical response). In the latter case, the occurrence of the non-

58 uniform shrinkage profiles has been only recently identified [19] and the ability to couple the  
59 hygro-thermo-chemical behaviour to its mechanical response will enable more accurate  
60 structural predictions associated to the serviceability limit state requirements of building floors.  
61 For these applications, the wider use of hygro-thermo-chemical-mechanical models for service  
62 design and modelling needs to be supported by techniques capable of adequately identifying the  
63 required material parameters, especially in applications where they can give useful insight into  
64 the structural problem. Not all material parameters to be specified in input in these hygro-thermo-  
65 chemical-mechanical models can be easily determined and, to better highlight this aspect, the  
66 model material parameters are subdivided into the following two sets: (i) one set of parameters  
67 that can be evaluated based on the concrete mix specifications or from data reported in the  
68 literature; and (ii) a second set of parameters characterised by a large variability (based on data  
69 available in the literature) and, among these, many parameters do not possess a precise physical  
70 meaning and, for this reason, are not amenable to a direct measurement.

71 In this context, the main contribution of this paper relies on the development of a robust inverse  
72 analysis procedure for the identification of the second set of material parameters (i.e. listed at  
73 point (ii) above) that are required in input for the use of the hygro-thermo-chemical-mechanical  
74 models. This paper contributes to this effort by proposing different strategies for the  
75 characterisation of the material parameters considering different exposure conditions.

76 In this work, the robustness of the proposed inverse analysis procedure is determined based on  
77 the use of pseudo-experimental results as input data (e.g. [23-25]) that includes measurements  
78 of temperature, relative humidity and total deformations. This data has been generated  
79 considering the same exposure conditions of commonly available reinforced or prestressed  
80 concrete slabs, i.e. exposed on both its surfaces, and of slabs exposed only from one side because  
81 sealed on its opposite side (e.g. composite slabs and industrial pavements). The proposed  
82 methodology is developed with the idea of minimising the number and the duration of the  
83 measurements to be carried out and of investigating how these are influenced by different

84 exposure conditions. After introducing the key features of the hygro-thermo-chemical-  
85 mechanical model considered in this study, the main outcomes and representative results  
86 obtained from an extensive sensitivity analysis are presented because providing insight into the  
87 most effective number, location and duration of the measurements to be used as input of the  
88 inverse analysis procedure. The basis of the inverse analysis procedure is then presented and its  
89 robustness is tested against selected scenarios constructed using pseudo-experimental data  
90 subjected to different degrees of noise and for different external temperatures and relative  
91 humidities surrounding the concrete. Representative results are reported in the paper to give  
92 insight into the use and effectiveness of the proposed methodology. These results are also  
93 expected to support the effective planning of the instrumentation setup to be used in experimental  
94 tests on service conditions performed in controlled laboratory environments and for the  
95 arrangement of in-situ monitoring and investigations, for example during construction or during  
96 day-to-day service operations, associated to applications whose service response is influenced  
97 by shrinkage.

## 98 **2. Hygro-thermo-chemical-mechanical model**

99 The hygro-thermo-chemical-mechanical model considered in this paper is able to predict the  
100 variations of the relative humidity  $h$ , temperature  $T$  and deformation  $\varepsilon$  that take place over time  
101 within the spatial domain  $\Omega$  of a concrete component taking into account its environmental  
102 conditions. The model here presented has been proposed in [13] and applied to a concrete mix  
103 without the presence of silica fume. The main features of the model and its numerical  
104 implementation are described in the following.

105 The principal chemical reaction occurring during hardening of a concrete mix is cement  
106 hydration, whose extent is here expressed through a scalar variable  $\alpha_c$ , computed as the ratio  
107 between the actual level of hydration  $X_c$  and its theoretical asymptotic value  $X_c^{\infty,th}$  achievable

108 under ideal hygro-thermal conditions. The maximum level of the reaction degree  
 109  $\alpha_c^\infty = X_c^\infty / X_c^{\infty,th}$  is usually smaller than one, i.e.  $\alpha_c^\infty < 1$ . According to [26], we may assume  
 110  $\alpha_c^\infty = (1.032w/c)/(0.194 + w/c)$ , in which  $w/c$  depicts the water-to-cement ratio. The variation  
 111 over time  $\alpha_c$  increases with relative humidity content and reduces while approaching its  
 112 asymptotic value  $\alpha_c^\infty$  as expressed by the following Arrhenius type equation:

$$\alpha_c = \frac{A_{c1} (A_{c2}/\alpha_c^\infty + \alpha_c) (\alpha_c^\infty - \alpha_c) e^{(-\eta_c \alpha_c / \alpha_c^\infty)}}{[1 + (a - ah)^b]} \cdot e^{(-\gamma_c/T)} \quad (1)$$

113 where  $\gamma_c = E_{ac}/R$ ,  $E_{ac}$  is the hydration activation energy and  $R$  represents the universal gas  
 114 constant. Parameters  $A_{c1}$ ,  $A_{c2}$  and  $\eta_c$  have no precise physical meaning and govern the so-called  
 115 normalized chemical affinity. The function  $b_h(h) = [1 + (a - ah)^b]^{-1}$  takes into account the  
 116 slowing of the hydration process when relative humidity decreases below a certain value (around  
 117 80%). Parameters  $a$  and  $b$  are usually taken equal to 7.5 and 4.0, respectively, (see [1]).

118 The total water content  $w$ , present in the concrete mix, is expressed as the sum of the evaporable  
 119 water  $w_e$  and the non-evaporable water  $w_n$ , the latter being the water chemically bonded by  
 120 cement hydration and expressed as  $w_n(\alpha_c) = k_c \alpha_c c$ , with  $c$  being the cement ratio content and  
 121  $k_c$  a material parameter that, according to [13] and references herein, can be assumed equal to  
 122 0.253. The evaporable water is expressed as a function of the relative humidity (sorption  
 123 isotherm curve) and of the degree of cement hydration  $\alpha_c$  as follows:

$$w_e(h, \alpha_c) = \kappa_{vg}^c \alpha_c c (1 - 1/\bar{e}_2) + [w_0 - 0.188 \alpha_c c - \kappa_{vg}^c \alpha_c c (1 - 1/\bar{e}_1)] \cdot \frac{\bar{e}_2 - 1}{\bar{e}_1 - 1} \quad (2)$$

124 in which  $w_0$  ( $= (w/c)c$ ) is the initial water content and it is assumed that  $\bar{e}_2 = e^{10(g_1\alpha_c^\infty - \alpha_c)h}$   
 125 and  $\bar{e}_1 = e^{10(g_1\alpha_c^\infty - \alpha_c)}$ . Equation (2) also depends on material parameters  $\kappa_{vg}^c$  and  $g_1$  that  
 126 govern the amount of water contained in the cement gel pores and the shape of the sorption curve,  
 127 respectively.

128 Starting from the consideration that  $w = w_e(h, \alpha_c) + w_n(\alpha_c)$ , the variation of the humidity field  
 129 over time and space is described by the combination of the Fick's law, expressing the flux of  
 130 water mass  $\mathbf{j}$  as proportional to the gradient of the relative humidity  $h$  (i.e.  $\mathbf{j} = -D_h \nabla h$ ) and the  
 131 water mass balance equation, e.g. [1,13]:

$$\frac{\partial w_e}{\partial h} \frac{\partial h}{\partial t} = \nabla \cdot [D_h \nabla h] - \left( \frac{\partial w_e}{\partial \alpha_c} + \frac{\partial w_n}{\partial \alpha_c} \right) \mathcal{Q}_c \quad \text{in } \Omega \quad (3)$$

132 In the above equation, the moisture permeability  $D_h$  depends on the relative humidity  $h$  and  
 133 temperature  $T$  as per the following expression [13,27]:

$$D_h(h, T) = \frac{D_1}{\left[ 1 + (D_1/D_0 - 1)(1-h)^n \right]} \cdot e^{(E_{ad}/RT_0 - E_{ad}/RT)} \quad (4)$$

134 in which  $T_0$  is the reference room temperature (assumed equal to 296°K),  $E_{ad}/R = 4700K$  (see  
 135 e.g. [1]), and parameters  $D_0$ ,  $D_1$  and  $n$  depend on the specific concrete mix.

136 The temperature field is described by the combination of the Fourier's law, expressing the heat  
 137 flux  $\mathbf{q}$  as a function of the temperature spatial gradient ( $\mathbf{q} = \lambda \nabla T$ ), and the enthalpy balance  
 138 equation as follows:

$$\rho c_i \frac{\partial T}{\partial t} = \nabla \cdot [\lambda \nabla T] + \mathcal{Q}_c \quad \text{in } \Omega \quad (5)$$

139 where  $T$  is the absolute temperature,  $\lambda$  is the heat conductivity assumed constant in the present  
 140 study,  $\rho$  and  $c_t$  depict the concrete mass density and the specific heat, respectively, and  $\dot{Q}_c$   
 141 represents the rate of heat generated by cement hydration, calculated as  $\dot{Q}_c = \alpha_c \dot{Q}_c^0$ , with  $Q_c^0$   
 142 being the total heat content per unit cement mass.

143 Equations (3) and (5) are coupled by their dependency on the degree of cement hydration  $\alpha_c$  as  
 144 well as by the moisture diffusion coefficient  $D_h$  that depends on both temperature and relative  
 145 humidity.

146 The relative humidity obtained with the hygro-thermo-chemical model is then associated to a  
 147 free shrinkage hydrostatic strain tensor by means of the following expression:

$$\dot{\varepsilon}_{sh} = k_{sh} \dot{h} \quad (6)$$

148 which defines a linear relationship between the rate of change over time of the free shrinkage  
 149 deformation  $\dot{\varepsilon}_{sh}$  and the corresponding rate of change of the relative humidity  $\dot{h}$  by means of  
 150 the coefficient  $k_{sh}$ . The value for  $k_{sh}$  is usually considered to remain constant for practical  
 151 applications (e.g. [6,15,28,29]) even if, in reality, it has been shown that its value varies with the  
 152 relative humidity, e.g. [16,30]. Values reported in literature for  $k_{sh}$  exhibit a large scatter,  
 153 ranging between  $5 \times 10^{-4}$  and  $3.5 \times 10^{-3}$  (e.g. [29,31]) and, because of this, the value for  $k_{sh}$  needs  
 154 to be calibrated for different concrete mixes. By performing a time integration of Equation (6),  
 155 the free shrinkage deformation can be expressed as:

$$\varepsilon_{sh}(t) = k_{sh} (h(t) - h(0)) \quad (7)$$

156 The hygro-thermo-chemical-mechanical relationships introduced in Equations (1-7) depend on  
 157 many parameters. Some of them, listed in the upper part of Table 1, can be evaluated based on  
 158 the concrete mix specifications or from well-known data reported in the literature. Other  
 159 parameters are affected by a large variability and, among these, some do not possess a precise

160 physical meaning. This set of parameters is reported in the lower part of Table 1 and their range  
161 of variation (obtained and derived from [13,14,31,32]) is collected in Table 2.

162 The numerical solution of the proposed hygro-thermo-chemical model is achieved with the finite  
163 element method by solving the following discretized equations:

$$\begin{cases} \mathbf{W}\dot{\mathbf{H}} + \mathbf{D}\mathbf{H} = \mathbf{F} \\ \mathbf{C}\dot{\mathbf{T}} + \mathbf{A}\mathbf{T} = \mathbf{Q} \end{cases} \quad (8)$$

164 where  $\mathbf{H}$  and  $\mathbf{T}$  depict unknown vectors that collect all nodal values (of the finite element  
165 discretization) of the relative humidity and temperature fields at each instant, while the system  
166 matrices are defined in Appendix A. The Dirichlet's boundary conditions (on  $h$  and  $T$ ) are  
167 directly enforced on the vectors  $\mathbf{H}$  and  $\mathbf{T}$ , while Cauchy's boundary conditions enter into the  
168 right end side of the equation, see [33]. The system described in Equation (8) is solved by  
169 applying an explicit algorithm based on the  $\theta$ -method [33,34].

170 The mechanical analysis of the problem is then carried out using standard structural analysis  
171 procedures. In particular, for the purpose of the simulations presented in this paper a time-  
172 dependent cross-sectional analysis is performed to account for the shrinkage effects evaluated  
173 with Equation (7) based on method of analysis widely accepted in the literature, e.g. [35].

174 The use of the proposed numerical model is illustrated in the following considering an  
175 unreinforced and unloaded concrete component with the following boundary conditions: (i) heat  
176 exchange can take place from its opposite surfaces; and (ii) two different sets of boundary  
177 conditions are considered for the relative humidity, i.e. one with both concrete surfaces exposed  
178 for drying (Figure 1a) and a second with only one surface exposed to dry and opposite surface  
179 sealed (Figure 1b). For ease of reference, these boundary conditions have been referred to as EE  
180 and ES, respectively, in Figure 1.

181 Representative results related to the humidity profiles are provided in Figures 2 and 3 at different  
182 time increments for a period of 10 years and considering two concrete thicknesses, namely



183 100 mm and 250 mm. The adopted concrete mix is typical of a normal-strength concrete and its  
184 specifications are presented in Table 3. The simulations have been performed considering two  
185 boundary conditions, i.e. exposed-exposed (Figure 1a) in Figures 2a and 3a as well as exposed-  
186 sealed (Figure 1b) in Figures 2b and 3b, and the model parameters are based on the mean values  
187 of the ranges included in Table 2 and on the values specified in Table 3. Results presented in  
188 Figures 2 and 3 have been calculated assuming a wet curing period of 10 days.

189 The results of Figures 2 and 3 highlight the ability of this model to simulate the highly nonlinear  
190 humidity profiles that can develop through the concrete thickness and how these can be  
191 influenced by the drying mechanism activated by the different external environmental  
192 conditions. In particular, the nonlinear variations of relative humidity illustrated in Figure 2 show  
193 that, when exposed to a dry environment (i.e. environmental relative humidity of 40%), the thin  
194 concrete component cannot approach an equilibrium condition through its entire thickness with  
195 the ambient conditions even after nearly 10 years from casting. In the case of the concrete  
196 component subjected to exposed-sealed environmental conditions, non-symmetric humidity  
197 distributions develop due to the inability of the concrete to dry from its sealed surface as shown  
198 in Figures 2b and 3b. For a thicker concrete component the moisture transport process is slower  
199 and requires more time than a thinner one in achieving a stationary solution. For example, after  
200 ten years of simulation the variation of relative humidity measured at mid height is smaller  
201 (Figure 3) than that occurring in the thinner specimen (Figure 2).

202 The corresponding free shrinkage profiles are determined by inserting the relative humidity  
203 distributions of Figures 2 and 3 into Equation (7) as shown in Figures 4 and 5 for thicknesses of  
204 100 mm and 250 mm, respectively. The consequent total deformations are then evaluated from  
205 a time-dependent cross-sectional analysis based on the calculated free shrinkage profiles (dot  
206 lines in Figures 4 and 5), widely used in the literature for the evaluation of the service response  
207 of concrete structures (e.g. [35]) and their variations (i.e. of calculated total deformations) are

208 also plotted in Figures 4 and 5 at different instants in time (see continuous lines). From a  
209 qualitative viewpoint, the total deformations induced in an exposed-exposed unreinforced  
210 concrete component by the nonlinear shrinkage are constant through its thickness and well reflect  
211 the simplifying assumption adopted in international concrete codes (e.g. [36,37]) that specify the  
212 use of a constant shrinkage distribution for design purposes. In the case of an exposed-sealed  
213 concrete component, the total deformations produced by the calculated humidity profile lead to  
214 the development of a non-uniform shrinkage distribution. This behaviour is typical of industrial  
215 pavements that can dry predominantly from their exposed upper surface (see e.g. [17,18]) and,  
216 as recently reported in the literature, of composite floor systems in which concrete slabs are cast  
217 on profiled steel sheeting and can only dry from the exposed surface (see e.g. [19,20,21,22]). As  
218 expected, free shrinkage and total deformations are larger when considering thinner components,  
219 as noted comparing Figures 4 and 5.

### 220 **3. Sensitivity analysis**

221 The sensitivity analysis is intended to compute the influence of each sought parameter on the  
222 measurable quantities and to support the design of the experiments for inverse analysis purposes.  
223 In particular, the sensitivity analysis is applied to gain a better understanding on how the sought  
224 material parameters, i.e. those listed in the lower part of Table 1, influence the variations of the  
225 total deformations over time in order to assist the selection of the most effective time duration  
226 and spatial positions to be considered for the proposed inverse analysis (see e.g., [25], [38]).  
227 A preliminary sensitivity study was carried out considering the hygro-thermo-chemical model  
228 applied to an exposed-exposed concrete component that highlighted the presence of two regions  
229 where the humidity measurements presented the highest sensitivities, i.e. at the concrete mid-  
230 height and a position close to the concrete surface (i.e. at about 10 mm from the external surface),  
231 for the first few months from casting, while the highest sensitivity for the temperature

232 distributions are noted at the mid-height of the concrete component in the first 6 hours from  
233 casting.

234 The sensitivity index is computed as partial derivative of the measured quantities, e.g. total  
235 deformation  $\varepsilon$ , with respect to the model parameters  $p_i$  at a certain time instant  $t$  and in a certain  
236 position  $z$  along the thickness of the concrete component as follows:

$$S_{\varepsilon, p_i}(z, t, \mathbf{p}) = \frac{\partial \varepsilon(\mathbf{p}, z, t)}{\partial p_i} \frac{p_i}{\varepsilon(\mathbf{p}, z, t)} \quad (9)$$

237 This index is normalised, for comparison purposes, with respect to both the parameter and the  
238 measured quantity value. In the numerical computations, the derivatives have been approximated  
239 by forward finite-differences with 0.1% increment, and have been evaluated at the top and  
240 bottom surfaces of the concrete component and for a certain number of time instants.

241 Figure 6 shows the sensitivity index, continuously varying in time and space, computed  
242 according to Equation (9), of the deformation profiles measured at the top and bottom surfaces  
243 of both exposed-exposed and exposed-sealed concrete components. In particular, the sensitivity  
244 index computed for the exposed-sealed (ES) concrete component appear to be generally higher  
245 than those determined for the exposed-exposed (EE) case. Under the ES boundary condition, the  
246 deformations measured at the sealed (bottom) surface generally show a higher sensitivity to the  
247 model parameters than that of the deformation measured at the exposed (top) surface.

248 All parameters governing cement hydration, namely  $A_{c2}$ ,  $\eta_c$  and  $\gamma_c$ , reach their highest  
249 sensitivity on the measured deformation profiles after a few days from casting, when this  
250 chemical reaction is more active, and the maximum value among these occurs for parameter  $\gamma_c$   
251 related to the hydration activation energy while sensitivity with respect to  $A_{c2}$  is almost  
252 negligible. It is also interesting to observe that the sensitivity of the deformation profile,  
253 measured at the sealed surface, with respect to the model parameters other than those governing  
254 cement hydration, reaches always its highest value in the first few months after casting, therefore

255 highlighting how, during this period, the experimental information collected are mostly bound  
256 to enhance the identifiability of the sought parameters.

257 Among the parameters governing moisture permeability, the one which most affects the  
258 deformation profiles is the exponent  $n$ , characterized by a sensitivity index greater than the ones  
259 computed for parameters  $D_0$  and  $D_1$ . Sensitivity with respect to  $\mathcal{Q}_c^{\circ}$  is almost negligible since  
260 this parameter is expected to influence primarily the variation of the temperature field.

261  
262 Figure 7 illustrates some representative sensitivity results obtained with respect to selected model  
263 parameters over a period of one year for concrete thicknesses of 100 mm and 250 mm. In  
264 particular, the thinner component exhibits an extremely high sensitivity for the deformation  
265 measured at its sealed (bottom) surface for about 30 days from casting, and the differences in  
266 sensitivity exhibited between the strains measured at the sealed (bottom) and exposed (top) sides  
267 of the thinner component are more pronounced than those calculated for the thicker component.

#### 268 **4. Inverse analysis**

269 The inverse problem is usually formulated as the minimization of the discrepancy between the  
270 experimental results and same quantities numerically computed as a function of the sought  
271 parameters.

272 The identifiability of the parameters contained in the hygro-thermo-chemical-mechanical model  
273 presented in Section 2 has been investigated following a numerical procedure already adopted in  
274 other studies (see e.g. [39,40,41]), which consists of the implementation of different inverse  
275 analysis exercises starting from the so-called pseudo-experimental results, i.e. results  
276 numerically generated from a given set of model parameters, supplied in input to the inverse  
277 problem, which, if well-posed, should provide in output the values of the parameters adopted to  
278 generate the pseudo-experimental data.

279 The input data consist of humidity and temperature profiles taken at different locations through  
280 the concrete thickness and at different time instants as well as the total deformations measured

281 at both sides of the concrete component after completion of the curing period. In particular, the  
 282 relative humidity  $h_{e,\tau s}$  is measured through the concrete component thickness in a discretised  
 283 number of locations  $s = 1K N_{hz}$  and for a certain number of time instants  $\tau = 1K N_{ht}$ . Similarly,  
 284 at each instant  $\tau = 1K N_{Tt}$ , the temperature distribution  $T_{e,\tau s}$  is measured through the thickness  
 285 of the component in a discretised number of points  $s = 1K N_{Tz}$ ; and at each instant  $\tau = 1K N_{et}$ ,  
 286 total deformation  $\varepsilon_{e,\tau s}$  is measured at the two sides (i.e. top and bottom) of the concrete  
 287 component. The choice of the discretization points adopted for both the space and time domains  
 288 is based on the outcomes of the sensitivity analysis.

289 In the present study all experimental information are processed together and uncertainties of both  
 290 experimental measurements and system modelling are not considered within a stochastic  
 291 framework, but the effect of random noise, applied to the inverse problem input data, is  
 292 accounted for to investigate the robustness of the proposed identification procedure.

293 Collecting the model parameters to be estimated (i.e. those listed in the lower part of Table 1) in  
 294 vector  $\mathbf{p}$ , and denoting experimental and computed quantities by subscripts “e” and “c”,  
 295 respectively, the discrepancy norm between measured and computed quantities can be expressed  
 296 as follows:

$$w(\mathbf{p}) = \phi_h \sum_{\tau} \sum_s^{N_{ht}} \left[ \frac{(h_{n,\tau s} - h_{e,\tau s})^2}{h_{e,\tau s}^2} \right] + \phi_T \sum_{\tau} \sum_s^{N_{Tz}} \left[ \frac{(T_{n,\tau s} - T_{e,\tau s})^2}{T_{e,\tau s}^2} \right] + \phi_{\varepsilon} \sum_{\tau} \sum_s^2 \left[ \frac{(\varepsilon_{n,\tau s} - \varepsilon_{e,\tau s})^2}{\varepsilon_{e,\tau s}^2} \right] \quad (10)$$

297 where  $\phi_h = 1/(N_{ht}N_{hz})$ ,  $\phi_T = 1/(N_{Tt}N_{Tz})$  and  $\phi_{\varepsilon} = 1/(2N_{et})$  are weight factors defined in order  
 298 to ensure an equivalent contribution of the three terms defining the objective function.

299 The minimization of the objective function in Equation (10) is performed by the Trust Region  
 300 (TR) algorithm (see, e.g. [42,43]). Starting from an assigned initialization vector, this is  
 301 automatically updated by means of an iterative procedure based on the minimization of a  
 302 quadratic approximation of the objective  $w(\mathbf{p})$  within a “trust” region, whose dimensions are

303 updated step by step based on the results of the previous iteration. The process is stopped by the  
 304 fulfilment of a priori tolerances on either the variation of the objective function or the Euclidean  
 305 norm of the normalized optimization variables.

306 For each adopted set  $\mathbf{p}^{ad}$  of the parameters model, pseudo-experimental data are generated and  
 307 perturbed by different noise extractions ( $n = 1 \dots N_{NOISE}$ ), generated with uniform probability  
 308 density over an interval centred on the exact value. For each noise extraction, the inverse problem  
 309 is solved several times ( $i = 1 \dots N_{INIT}$ ) starting from different initialization vectors, to check the  
 310 occurrence of local minima that might exist in view of the nonlinear and non-convex nature of  
 311 the objective function. For a given noise extraction the identified value  $\mathbf{p}_n^{id}$  is computed as  
 312 average of all values  $\mathbf{p}_{ni}^{id}$  identified in relation to the different initializations, weighted with  
 313 respect to the inverse of the objective function in solution, as:

$$\mathbf{p}_n^{id} = \sum_i^{N_{INIT}} \mathbf{p}_{ni}^{id} \chi_i / \sum_i^{N_{INIT}} \chi_i, \quad \chi_i = 1/w(\mathbf{p}_{ni}^{id}) \quad (11)$$

314 The identification error for each model parameter  $k$  is then computed as:

$$err_{n,k}^{id} = 100 \cdot \left| \frac{p_{n,k}^{id} - p_k^{ad}}{p_k^{ad}} \right| \quad (12)$$

315 A final measure of the identifiability error of each sought parameter is defined in terms of average  
 316 of all the single errors, computed for each noise extraction:

$$err_k^{id} = \frac{1}{N_{NOISE}} \sum_n^{N_{NOISE}} err_{n,k}^{id} \quad (13)$$

317 with  $err_{n,k}^{id}$  being defined as absolute value, see equation (12), to avoid compensations between  
 318 errors of opposite signs when a large number of random noise extractions is adopted.

## 319 **4.1 Results**

320 Different inverse analysis exercises have been solved in the following to investigate the optimal  
 321 formulation of the inverse problem for the full identification of the parameters listed in the lower

322 part of Table 1, i.e. those characterised by a large variability or not amenable to direct  
323 measurement for the lack of a precise physical meaning. As input data to the inverse problem,  
324 humidity, temperature and deformation profiles' measurements have been considered. In the  
325 following, only representative results are presented to outline and support the key findings of  
326 this work.

327 The concrete properties included in the simulations correspond to the mean values reported in  
328 Table 2 and those specified in Table 3. The external temperature has been assumed constant and  
329 equal to 20°C. In all simulations, a random noise of 10% has been applied to the numerically  
330 generated pseudo-experimental data used in input.

331 The first inverse analysis simulations highlighted how the inverse problem is not well posed for  
332 the concurrent identification of parameters  $A_{c1}$  and  $\gamma_c$ . This lack of identifiability is attributed  
333 to the form in which these parameters appear in Equation (1) for the evaluation of the rate of  
334 cement hydration reaction  $\alpha_c$ . In this equation, both parameters have an equivalent effect on  
335  $\alpha_c$ , i.e. an increase in  $A_{c1}$  leads to an increase of  $\alpha_c$  that could be similarly produced by a  
336 decrease of  $\gamma_c$ . Because of this, the inverse analysis procedure cannot distinguish between these  
337 two parameters and, in view of a much higher sensitivity of  $\gamma_c$ , the following inverse analysis  
338 exercises will be carried out assuming  $A_{c1}$  known a priori while still identifying  $\gamma_c$ . The validity  
339 of this assumption is later confirmed by the results outlining how the adoption of different a  
340 priori values for  $A_{c1}$  does not jeopardize the identifiability of the sought parameters.

341 Table 4 reports the results obtained considering a 100 mm thick concrete component wet cured  
342 for 1 day from casting, exposed to an ambient relative humidity equal to 40% and assuming  
343 different boundary conditions. The number of discrete humidity measurements through the  
344 thickness of the concrete component have been varied and the inclusion of a temperature  
345 measurement has been considered. The measurements are performed for a period of 30 days  
346 (with a frequency of one measurement per hour). Columns A, B, C and D in Table 4 provide the

347 results obtained under exposed-exposed (denoted as EE) conditions (Figure 1a) and highlight the  
348 need to use two relative humidity measurements (column D) to ensure the identifiability of all  
349 parameters (with identified errors' magnitude within the noise level introduced in the pseudo-  
350 experimental data). By using one relative humidity measurement, for example located at 50 mm  
351 (Column B) or 10 mm (Column C) from the external concrete surface, or without monitoring  
352 relative humidity (Column A), the information provided as input of the inverse problem is not  
353 sufficient for the identification of all sought parameters, because the estimation of  $D_0$  or  $D_1$   
354 produces an error (at its maximum of 36.5%) that is larger than the magnitude of the added noise.  
355 For an exposed-sealed (referred to as ES) concrete component, column E shows that the  
356 experimental information consisting of one temperature and both surface deformation  
357 measurements are sufficient to guarantee the identifiability of all parameters. The inclusion of  
358 one relative humidity measurement for the ES conditions, for example located at the component  
359 mid-height, does not improve significantly the results as depicted by the values reported in  
360 column F of Table 4. Columns G and H highlight that, without the inclusion of a temperature  
361 measurement, the identification procedure does not lead to a successful characterisation of  $\mathcal{Q}_c^{\%}$   
362 and  $A_{c2}$  when considering both EE and ES exposure conditions. These observations highlight  
363 how the use of a temperature measurement as experimental information is crucial for the  
364 identification of the model parameters governing cement hydration that cannot be identified if  
365 information on deformation or relative humidity only are considered.

366 The results discussed above have been obtained for a relatively thin concrete component with a  
367 thickness of 100 mm. In the case of a 250 mm thick component, representative errors are  
368 presented in Table 5. In this case, a longer period of measurements, of at least 60 days, is needed  
369 for the exposed-exposed case (as depicted in Columns B and C) to collect the amount of  
370 experimental information needed for the calibration of the model parameters, especially of those  
371 governing the moisture permeability. Shorter monitored periods (reported in column A for



372 30 days) do not provide sufficient experimental information for the identification. For an  
373 exposed-sealed concrete component, differently from the 100 mm thickness, temperature and  
374 deformation profiles are not sufficient for the present identification purposes (see columns D and  
375 E), and one humidity measurement taken at mid-height is necessary to make the inverse problem  
376 well posed (see columns F and G). This is here attributed to the fact that, as shown in Figure 7,  
377 the sensitivity of the deformation measurements at the sealed concrete surface of a thicker  
378 component is much lower than the corresponding value obtained for a thinner component. As a  
379 consequence, the experimental information obtained from a thicker component is not sufficient  
380 for the definition of a well-posed inverse problem without the use of humidity measurements.  
381 This consideration is confirmed by the results reported in Table 6, where it is shown that for an  
382 increasing concrete component thickness (varying from 100 mm to 400 mm in columns A to D),  
383 the parameter  $\kappa_{vg}^c$  is identified with an increasing error. For the thicknesses considered in  
384 columns B-D, it is necessary to include at least one relative humidity measurement, for example  
385 placed at the concrete mid-height, to ensure the identifiability of all model parameters as depicted  
386 in columns F-H.

387 At the beginning of this section, it has been discussed that the parameters  $A_{c1}$  and  $\gamma_c$  could not  
388 be uniquely identified. For this reason, the inverse methodology followed in this study consisted  
389 in assigning an a priori value to  $A_{c1}$  equal to its mean value reported in the literature ( $=29450 \text{ s}^{-1}$   
390 based on the range provided in Table 2), i.e. the same value adopted in generating the pseudo-  
391 experimental data. Table 7 reports the results of some inverse analysis exercises when an  
392 incorrect value for  $A_{c1}$  (i.e. different from the one used for the generation of the pseudo-  
393 experimental data) is specified in input of the inverse analysis. In particular, the upper and lower  
394 limits of  $A_{c1}$  (as specified in Table 2) are used for the results reported in columns B and C  
395 considering the EE conditions and in columns E and F for the ES conditions, while columns A  
396 and D depict the errors determined using the exact value for  $A_{c1}$  (i.e. the value adopted to

397 generate pseudo-experimental data). These results confirm that the identifiability of all  
398 parameters is not affected by an incorrect assumption of  $A_{c1}$ , except for the “companion”  
399 parameter  $\gamma_c$ , whose identification error increases, especially when the lower limit is assumed  
400 (however always within the order of magnitude of the added noise for the cases considered).

401 The inverse analysis cases proposed for the exposed-exposed and exposed-sealed conditions are  
402 revisited in the following assuming sinusoidal time-varying boundary conditions expressed in  
403 terms of external temperature and relative humidity applied to the concrete surfaces. Only  
404 selected case studies (taken from Tables 4 and 5) are considered in the following with the  
405 sinusoidal boundary conditions. In particular, columns A and C in Table 8 correspond to columns  
406 E and D in Table 4, respectively; while columns D and E correspond to columns B and F in  
407 Table 5, respectively. Based on these results, the optimal (in terms of minimum measurements  
408 to be taken) experimental setups studied for the 250 mm thick concrete component under external  
409 constant boundary conditions (Table 5) are still effective for the identification of the sought  
410 material parameters in the case of sinusoidally-varying boundary conditions, see columns D and  
411 E in Table 8. For the thinner specimen, some problems arise (with the varying boundary  
412 conditions) in relation to the identification of the parameter  $A_{c2}$ . In particular, column A in Table  
413 8 shows that for the case of the exposed-sealed specimen the error increases (when compared to  
414 the case with constant boundary conditions) but it remains of the same order and magnitude of  
415 the added noise. It has been observed that this error can be further reduced by adding a  
416 temperature measurement close to the external surface (see column B in Table 8). The  
417 combination of the small thickness and of the exposed-exposed boundary conditions maximizes  
418 the influence of the time-varying boundary conditions on the measurements taken inside the  
419 specimen and induces the largest identification error of the parameter  $A_{c2}$ , as reported in column  
420 C (Table 8), however, without jeopardizing the identification of the other parameters.

## 421 **5. Conclusions**

422 This paper has focussed on the identifiability of the parameters required for a hygro-thermo-  
423 chemical-mechanical model that predicts variations of temperature, relative humidity and  
424 shrinkage induced deformations in concrete components. In particular, the model parameters  
425 have been subdivided into two main sets: (i) one set of parameters that can be evaluated on the  
426 basis of the concrete mix specifications or from literature data; and (ii) a second set of parameters  
427 that are characterised by a large variability and, in some cases, without a precise physical  
428 meaning, are not amenable to a direct measurement. This paper has proposed an inverse analysis  
429 procedure for the identification of the model parameters contained in this second set by  
430 considering different concrete exposure conditions and by using following variables as input  
431 data: total deformations at the concrete surfaces, temperature and relative humidity profiles in  
432 some positions inside the concrete component. These results may find applications in enhancing  
433 the design of in-situ investigations and of experimental tests, and in minimising the necessary  
434 collected experimental information (in terms of monitored period and number of discrete  
435 temperature and relative humidity measurements). The outcomes of the different inverse  
436 analyses' exercises have been considered successful when all parameters have been identified  
437 with an error smaller than the noise added to the pseudo-experimental data in input to the inverse  
438 problem. The boundary conditions included in this study are described as follows: (i) heat  
439 transfer has been assumed to take place through both concrete surfaces; and (ii) two exposure  
440 conditions have been considered for the relative humidity, i.e. one assuming both concrete  
441 surfaces to be exposed for drying (referred to as EE) and one where only one surface has been  
442 exposed with the remaining one being sealed (denoted as ES). The identification process has  
443 been applied considering different environments of external temperature and relative humidity  
444 surrounding the concrete.

445 Based on the results and case studies considered in this paper, it is possible to draw the  
446 conclusions listed below.

- 447 • For concrete components, subjected to constant boundary conditions (i.e. constant  
448 external temperature and relative humidity) and exposed on both sides (EE conditions),  
449 the minimum measurements required for the identification of all model parameters  
450 consist of relative humidities taken at two locations within the concrete thickness (e.g.  
451 one at the mid-height and one close to the surface), one temperature reading at mid-height  
452 and total deformation at the concrete surface.
- 453 • Concrete components, exposed to constant environmental conditions, sealed on one side  
454 and allowed to dry on the opposite one (ES conditions) require varying strategies  
455 depending on their thickness. For thinner components (here taken as 100 mm thick), all  
456 model parameters are identifiable by monitoring the total deformations at both the  
457 concrete surfaces and temperature at mid-height. For larger components, additional  
458 measurements related to relative humidity need to be included in the input data of the  
459 inverse analysis procedure.
- 460 • For concrete components exposed to sinusoidally-varying environmental conditions (i.e.  
461 varying external temperature and relative humidity), the inverse analysis requires the use  
462 of the measured external temperature and relative humidity variations as input data of the  
463 direct operator. It has been observed that for relatively large concrete thicknesses (here  
464 taken as 250 mm), the same minimum experimental information required for a concrete  
465 specimen exposed to constant boundary conditions is sufficient for the identification of  
466 the sought material parameters, while for thinner concrete components (here taken as  
467 100 mm) the use of the same approach leads to larger error for only one parameter  
468 (associated with the variation of the degree of cement hydration over time) without  
469 jeopardizing the identification of the remaining parameters.

470 **6. Acknowledgements**

471 The work in this article was supported under the Australian Research Council's Discovery  
 472 Projects funding scheme (project number DP140400529).

473 **Appendix A**

474 Matrices and vectors of the system in equation (8) are defined as follows:

$$\mathbf{W} = \bigcup_e \int_{\Omega_e} \mathbf{N}_e^T \frac{\partial w_e}{\partial h} \mathbf{N}_e d\Omega \quad (\text{A1})$$

$$\mathbf{D} = \bigcup_e \int_{\Omega_e} \mathbf{B}_e^T D_h \mathbf{B}_e d\Omega \quad (\text{A2})$$

$$\mathbf{F} = -\bigcup_e \int_{\Gamma_e} \mathbf{N}_e^T \mathbf{n}^T \mathbf{j} d\Gamma - \bigcup_e \int_{\Omega_e} \mathbf{N}_e^T \left( \frac{\partial w_e}{\partial \alpha_c} + \frac{\partial w_n}{\partial \alpha_c} \right) \mathcal{C}_c d\Omega \quad (\text{A3})$$

$$\mathbf{C} = \bigcup_e \int_{\Omega_e} \mathbf{N}_e^T \rho c_i \mathbf{N}_e d\Omega \quad (\text{A4})$$

$$\mathbf{\Lambda} = \bigcup_e \int_{\Omega_e} \mathbf{B}_e^T \lambda \mathbf{B}_e d\Omega \quad (\text{A5})$$

$$\mathbf{Q} = -\bigcup_e \int_{\Gamma_e} \mathbf{N}_e^T \mathbf{n}^T \mathbf{q} d\Gamma + \bigcup_e \int_{\Omega_e} \mathbf{N}_e^T \mathcal{C}_c d\Omega \quad (\text{A6})$$

475 where symbol  $\bigcup_e$  refers to the assembly operation typical of the finite element approach, and

476 matrices  $\mathbf{N}_e$  and  $\mathbf{B}_e$  collect shape functions and their spatial derivatives, respectively.

477

478 **References**

- 479 [1] Z.P. Bažant, L.J. Najjar, Nonlinear water diffusion in nonsaturated concrete, *Materiaux et*  
480 *Constructions* 5 (1972) 3–20.
- 481 [2] F.J. Ulm, O. Coussy, Modeling of thermo-chemical–mechanical couplings of concrete at  
482 early age, *Journal of Engineering Mechanics ASCE* 121 (1995) 785–794.
- 483 [3] M. Cervera, J. Oliver, T. Prato, Thermo–chemo–mechanical model for concrete. I: hydration  
484 and aging, *Journal of Engineering Mechanics ASCE* 125 (1999) 1018–1027.
- 485 [4] D. Gawin, F. Pesavento, B.A. Schrefler, Hygro-thermo-chemo-mechanical modelling of  
486 concrete at early ages and beyond, Part I: hydration and hygrothermal phenomena, *International*  
487 *Journal Numerical Methods Engineering* 67 (2006) 299–331.
- 488 [5] M. Du, X. Jin, H. Ye, N. Jin, Y. Tian, A coupled hygro-thermal model of early-age concrete  
489 based on micro-pore structure evolution, *Construction and Building Materials* 111 (2016) 689–  
490 698.
- 491 [6] T. Gasch, R. Malm, A. Ansell, A coupled hygro-thermo-mechanical model for concrete  
492 subjected to variable environmental conditions, *International Journal of Solids and Structures*  
493 91 (2016) 143–156.
- 494 [7] J.K. Kim, C.S. Lee, Moisture diffusion of concrete considering self-desiccation at early ages,  
495 *Cement and Concrete Research* 29 (1999) 1921–1927.
- 496 [8] B.H. Oh, S.W. Cha, Nonlinear analysis of temperature and moisture distributions in early-  
497 age concrete structures based on degree of hydration, *ACI Materials Journal* 100 (2003) 361–70.
- 498 [9] S. Rahimi-Aghdama, Z.P. Bažant, M.J. Abdolhosseini Qomic, Cement hydration from hours  
499 to centuries controlled by diffusion through barrier shells of C-S-H, *Journal of the Mechanics*  
500 *and Physics of Solids* 99 (2017) 211–224.

- 501 [10] S.D. Abyaneh, H.S. Wong, N.R. Buenfeld, Modelling the diffusivity of mortar and concrete  
502 using a three-dimensional mesostructure with several aggregate shapes, *Computational Materials*  
503 *Science* 78 (2013) 63–73.
- 504 [11] S.D. Abyaneh, H.S. Wong, N.R. Buenfeld, Simulating the effect of microcracks on the  
505 diffusivity and permeability of concrete using a three-dimensional model, *Computational*  
506 *Materials Science* 119 (2016) 130–143.
- 507 [12] S.B. Tang, Q.L. Yu, H. Li, C.Y. Yu, C.Y. Bao, C.A. Tang, Mesomechanical model of  
508 moisture diffusion and shrinkage cracking in building material – Model development,  
509 *Construction and Building Materials* 47 (2013) 511–529.
- 510 [13] G. Di Luzio, G. Cusatis, Hygro-thermo-chemical modeling of high performance concrete.  
511 I: Theory, *Cement & Concrete Composites* 31 (2009) 301–308.
- 512 [14] G. Di Luzio, G. Cusatis, Hygro-thermo-chemical modeling of high performance concrete.  
513 II: Numerical implementation, calibration, and validation, *Cement & Concrete Composites* 31  
514 (2009) 309–324.
- 515 [15] P. Havlásek, M. Jirásek, Multiscale modeling of drying shrinkage and creep of concrete,  
516 *Cement and Concrete Research* 85 (2016) 55–74.
- 517 [16] F.H. Wittmann, Creep and shrinkage mechanics, in: Z.P. Bažant, F.H. Wittmann (Eds.),  
518 *Creep and Shrinkage of Concrete Structures*, John Wiley & Sons Ltd., 1982, pp. 129–161.
- 519 [17] ACI (2006) ACI 302.2R-06 Guide for Concrete Slabs that Receive moisture-sensitive  
520 flooring materials, American Concrete Institute.
- 521 [18] H.J. Oh, Y.K. Cho, Y. Seo, S.-M. Kim, Experimental analysis of curling behaviour of  
522 continuously reinforced concrete pavement, *Construction and Building Materials* 128 (2016) 57–  
523 66.

- 524 [19] G. Ranzi, G. Leoni, R. Zandonini, State of the art on the time-dependent behaviour of  
525 composite steel-concrete structures, *Journal of Constructional Steel Research* 80 (2013) 252–  
526 263.
- 527 [20] G. Ranzi, Service design approach for composite steel-concrete floors, *Proceedings of the*  
528 *Institution of Civil Engineers: Structures and Buildings*, <https://doi.org/10.1680/jstbu.16.00196>.
- 529 [21] Q. Wang, G. Ranzi, Y. Wang, Y. Geng, Long-term behaviour of simply-supported steel-  
530 bars truss slabs with recycled coarse aggregate, *Construction and Building Materials* 116 (2016)  
531 335–346.
- 532 [22] R.I. Gilbert, M.A. Bradford, A. Gholamhoseini, Z.-T. Chang, Effects of Shrinkage on the  
533 Long-Term Stresses and Deformations of Composite Concrete Slabs, *Engineering Structures* 40  
534 (2012) 9–19.
- 535 [23] H.D. Bui, *Inverse Problems in the Mechanics of Materials: an Introduction*, CRC Press,  
536 Boca Raton FL, 1994.
- 537 [24] Z. Mroz, G.E. Stavroulakis, *Identification of Materials and Structures*, CISM Lecture Notes,  
538 Vol. 469, Springer-Verlag, Wien, 2005.
- 539 [25] G. Stavroulakis, G. Bolzon, Z. Waszczyszyn, L. Ziemianski, Inverse analysis, in: B.  
540 Karihaloo, R.O. Ritchie, I. Milne (Eds.), *Comprehensive Structural Integrity*, Elsevier Science  
541 Ltd., Kidlington (Oxfordshire), UK, 2003.
- 542 [26] S.J. Pantazopoulou, R.H Mills, Microstructural aspects of the mechanical response of plain  
543 concrete, *ACI Materials Journal* 92 (1995) 605–616.
- 544 [27] M. Jooss, H.W. Reinhardt, Permeability and diffusivity of concrete as function of  
545 temperature, *Cement Concrete Research* 32 (2002) 1497–1504.
- 546 [28] F. Benboudjema, F. Meftah, J.M. Torrenti, Interaction between drying, shrinkage, creep and  
547 cracking phenomena in concrete, *Engineering Structures* 27 (2005) 239–250.



- 548 [29] M. Jirásek, P. Havlásek, Microprestress–solidification theory of concrete creep:  
549 Reformulation and improvement, *Cement and Concrete Research* 60 (2014) 51–62.
- 550 [30] M. Azenha, C. Sousa, R. Faria, A. Neves, Thermo–hygro–mechanical modelling of self-  
551 induced stresses during the service life of RC structures, *Engineering Structures* 33 (2011) 3442–  
552 3453.
- 553 [31] G. Di Luzio, G. Cusatis, Solidification–microprestress–microplane (SMM) theory for  
554 concrete at early age: Theory, validation and application, *International Journal of Solids and*  
555 *Structures* 50 (2013) 957–975.
- 556 [32] L. Wan, R. Wendner, B. Liang, G. Cusatis, Analysis of the behavior of ultra high  
557 performance concrete at early age, *Cement and Concrete Composites* 74 (2016) 120–135.
- 558 [33] A. Quarteroni, *Modellistica numerica per problemi differenziali*, Springer-Verlag Italia,  
559 Milano, 2000.
- 560 [34] R. D. Cook, D. S. Malkus, M. E. Plesha, R. J. Witt, *Concepts and applications of finite*  
561 *element analysis*, 4<sup>th</sup> Edition, Wiley, 2002.
- 562 [35] R.I. Gilbert, G. Ranzi, *Time-dependent behaviour of concrete structures*, Spon Press,  
563 London, UK, 2011.
- 564 [36] EN 1992-1-1, *Eurocode 2: Design of concrete structures - Part 1-1: General rules and rules*  
565 *for buildings*, European Committee for Standardization, 2004.
- 566 [37] AS3600, *Australian Standard for Concrete Structures AS3600–2009*, Standards Australia,  
567 2009.
- 568 [38] M. Kleiber, H. Antúnez, T.D. Hien, P. Kowalczyk, *Parameter Sensitivity in Nonlinear*  
569 *Mechanics, Theory and Finite Element Computations*, John Wiley & Sons, Chichester, 1997.

570 [39]. M. Bocciarelli, V. Buljak, C.K.S. Moy, S.P. Ringer, G. Ranzi, An inverse analysis approach  
571 based on a POD direct model for the mechanical characterization of metallic materials,  
572 Computational Materials Science 95 (2014) 302–308.

573 [40] G. Bolzon, M. Talassi, An effective inverse analysis tool for parameter identification of  
574 anisotropic material models, International Journal of Mechanical Sciences 77 (2013) 130–144.

575 [41] R. Ardito, G. Cocchetti, Statistical approach to damage diagnosis of concrete dams by radar  
576 monitoring: Formulation and a pseudo-experimental test, Engineering Structures 28 (2006)  
577 2036–2045.

578 [42] T.F. Coleman, Y. Li, SIAM Journal of Optimization 6 (1996) 418–445.

579 [43] The Math Works Inc, USA, User’s Guide and Optimization Toolbox, Release 6.13, Matlab  
580 2004.

581

582  
583

Table 1. Material parameters required in input of the hygro-thermo-chemical-mechanical model.

	Parameter	Description
Parameters calculated based on concrete mix specifications or assigned known values well accepted in the literature	$c$	cement content
	$w/c$	water-to-cement ratio
	$a, b$	parameters associated with the variation of the degree of cement hydration over time and taken as $a = 7.5$ and $b = 4.0$ [1]
	$\lambda$	heat conductivity
	$\rho$	concrete mass density
	$c_t$	concrete specific heat
	$k_c$	parameter associated with non-evaporable water and taken as 0.253 (as suggested in [13])
Parameters characterised by a large variability (see Table 2) – some of which do not possess a precise physical meaning (to be identified with the inverse analysis presented in Section 4)	$A_{c1}, A_{c2}, \eta_c$	parameters with no precise physical meaning associated with the variation of the degree of cement hydration over time
	$\gamma_c$	parameter calculated as the ratio of the hydration activation energy over the universal gas constant
	$\mathcal{Q}_c$	total heat content per unit cement mass due to cement hydration
	$\kappa_{vg}^c$	parameter that governs the amount of water contained in the cement gel pores
	$g_1$	parameter that governs the shape of the sorption curve
	$D_0, D_1, n$	parameters that control the moisture permeability and depend on the specific concrete mix
	$k_{sh}$	parameter that relates the change over time of the free shrinkage deformation to the rate of the relative humidity

584

585

586

Table 2. Range of variation for the parameters listed in the lower part of Table 1.

Parameter	Range of variation	Mean value
$A_{c1}$	3900 – 55000 [s <sup>-1</sup> ]	29450
$A_{c2}$	10 <sup>-6</sup> – 5·10 <sup>-2</sup>	2.5·10 <sup>-2</sup>
$\eta_c$	5.5 – 8.0	6.75
$\gamma_c$	3000 – 8000 [K]	5500
$\mathcal{Q}_c^6$	400 – 550 [kJ/kg]	475000
$\kappa_{vg}^c$	0.10 – 0.26	0.18
$g_1$	1.20 – 2.20	1.70
$D_0/c$	0.2·10 <sup>-14</sup> – 7.5·10 <sup>-14</sup> [m <sup>2</sup> /s]	3.85·10 <sup>-14</sup>
$D_1/c$	4.8·10 <sup>-10</sup> – 12·10 <sup>-10</sup> [m <sup>2</sup> /s]	8.4·10 <sup>-10</sup>
$n$	3.0 – 4.5	3.75
$k_{sh}$	5×10 <sup>-4</sup> – 3.5×10 <sup>-3</sup>	2.0×10 <sup>-3</sup>

587

588

589 Table 3. Specifications of the concrete mix and some parameters used in the numerical  
590 simulations.

Parameter	Assumed value
$c$	312 kg/m <sup>3</sup>
$w/c$	0.57
$\lambda$	2.3 W/m°C
$\rho$	2400 kg/m <sup>3</sup>
$c_t$	1100 J/kg°C
$k_c$	0.253

591

592

593

594

595 Table 4. Results of the inverse analysis exercises in terms of  $err_k^{id}$  [%] by varying: boundary  
 596 conditions and location of discrete measurements for the relative humidity  $h$  and the  
 597 temperature  $T$ .

D	100 mm							
RH	40%							
Period of wet curing	1 day							
Period monitored	30 days							
Added noise	10%							
Boundary conditions	EE				ES		EE	ES
Location of discrete measurements <sup>1</sup> for $h$ [mm]	/	50	10	50/10	/	50	50/10	50/10
Location of discrete measurements <sup>1</sup> for $T$ [mm]	50				50		/	/
Column	A	B	C	D	E	F	G	H
$D_0$	8.5	36.5	10.6	8.7	4.1	2.3	2.7	2.0
$D_1$	13.7	5.9	4.8	6.4	1.9	1.3	2.1	0.8
$n$	2.8	4.4	0.9	0.7	0.4	0.5	0.4	0.3
$\kappa_{vg}^c$	8.0	8.8	6.8	9.6	3.1	3.9	4.6	3.7
$g_l$	7.2	5.0	5.2	8.2	1.4	0.6	3.0	1.1
$\gamma_c$	0.1	0.1	0.1	0.1	0.2	0.2	0.2	0.6
$\mathcal{Q}_c^{\circ}$	6.1	3.7	3.7	4.2	1.9	1.2	13.3	6.8
$A_{c2}$	8.2	5.3	6.2	8.1	3.8	2.8	4.9	12.2
$\eta_c$	8.9	5.2	5.1	6.1	2.6	1.6	2.4	0.9
$k_{SH}$	8.0	2.2	0.6	0.6	1.3	0.3	0.3	1.2

598 NOTE: <sup>1</sup>Locations measured from external surfaces of concrete component [mm].

599

600

601

602

603

604 Table 5. Results of the inverse analysis exercises in terms of  $err_k^{id}$  [%] by varying: boundary  
 605 conditions, location of discrete measurements for the relative humidity  $h$  and period monitored.

D	250 mm						
Location of discrete measurements for $T$	125 mm						
RH	40%						
Period of wet curing	1 day						
Added noise	10%						
	Boundary conditions			EE		ES	
Location of discrete measurements for $h$ [mm]	125/10			/		125	
Period monitored [days]	30	60	90	60	90	60	90
Column	A	B	C	D	E	F	G
$D_0$	14.5	6.1	2.3	5.3	8.1	6.8	4.8
$D_1$	3.0	1.8	2.4	2.4	3.5	3.2	3.1
$n$	2.2	1.0	0.4	0.9	1.2	1.1	0.8
$\kappa_{vg}^c$	10.3	6.0	6.2	11.8	19.0	8.2	7.1
$g_l$	3.5	1.8	2.3	2.6	5.3	2.3	1.9
$\gamma_c$	0.1	0.1	0.1	0.2	0.2	0.1	0.2
$\mathcal{Q}_c^{\%}$	1.4	1.0	1.2	0.7	1.7	0.8	1.1
$A_{c2}$	2.8	3.3	4.5	6.2	4.6	4.7	4.8
$\eta_c$	1.7	1.0	1.0	1.7	2.0	1.5	0.8
$k_{SH}$	0.5	0.2	0.2	1.3	2.2	0.2	0.2

606 NOTE: <sup>1</sup>Locations measured from external surfaces of concrete component [mm].

607  
 608  
 609

610 Table 6. Results of the inverse analysis exercises in terms of  $err_k^{id}$  [%] for an exposed-sealed  
 611 specimen by varying: location of discrete measurements for the relative humidity  $h$  and  
 612 component thickness  $D$ .

Location of discrete measurements for $T$	0.5×D							
RH	40%							
Period of wet curing	1 day							
Period monitored	90 days							
Added noise	10%							
	Boundary conditions				ES			
Location of discrete measurements for $h$ [mm]	/				0.5×D			
D [mm]	100	200	300	400	100	200	300	400
Column	A	B	C	D	E	F	G	H
$D_0$	3.2	5.8	7.2	8.4	4.9	3.0	6.6	6.8
$D_1$	1.7	1.9	2.9	6.4	1.6	2.1	3.5	5.2
$n$	0.4	0.7	1.0	1.4	0.3	0.5	1.0	1.1
$\kappa_{vg}^c$	5.3	14.3	18.6	20.5	5.1	6.0	7.5	9.4
$g_1$	1.2	3.5	5.3	5.9	1.6	1.5	2.0	2.7
$\gamma_c$	0.1	0.2	0.2	0.2	0.1	0.2	0.2	0.2
$\mathcal{G}_c^{\circ}$	1.0	1.5	1.5	1.4	0.9	1.1	1.1	1.1
$A_{c2}$	2.5	4.2	5.5	5.8	2.9	4.1	5.3	5.8
$\eta_c$	1.6	1.6	1.5	1.5	1.3	0.8	0.8	0.8
$k_{SH}$	0.7	1.7	2.2	1.8	0.2	0.2	0.2	0.3

613 NOTE: <sup>1</sup>Locations measured from external surfaces of concrete component [mm].

614

615



616 Table 7. Results of the inverse analysis exercises in terms of  $err_k^{id}$  [%] by varying: boundary  
 617 conditions, location of discrete measurements for the relative humidity  $h$  and assuming  
 618 different a-priori values for the parameter  $A_{c1}$ .

D	100 mm					
Location of discrete measurements for $T$	50 mm					
RH	40%					
Period of wet curing	1 day					
Period monitored	30 days					
Added noise	10%					
Boundary conditions	EE			ES		
Location of discrete measurements <sup>1</sup> for $h$ [mm]	50/10			50		
Parameter $A_{c1}$ [ $s^{-1}$ ]	29450	3900	55000	29450	3900	55000
Column	A	B	C	D	E	F
$D_0$	8.7	9.0	9.0	2.3	3.4	2.4
$D_1$	6.4	5.6	5.5	1.3	0.8	1.3
$n$	0.7	0.6	0.6	0.5	0.3	0.6
$\kappa_{vg}^c$	9.6	6.1	6.1	3.9	2.8	4.1
$g_l$	8.2	7.1	7.0	0.6	0.9	0.6
$\gamma_c$	0.1	10.8	3.3	0.2	10.5	3.4
$\mathcal{Q}_c^{\phi}$	4.2	4.5	4.4	1.2	0.8	1.1
$A_{c2}$	8.1	7.2	7.0	2.8	1.5	3.2
$\eta_c$	6.1	6.8	6.7	1.6	1.2	1.6
$k_{SH}$	0.6	0.3	0.3	0.3	0.4	0.5

619 NOTE: <sup>1</sup>Locations measured from external surfaces of concrete component [mm].

620

621

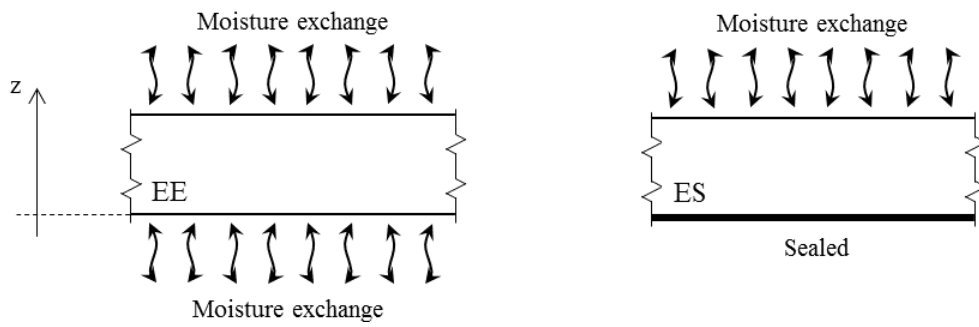
622

623 Table 8. Results of the inverse analysis exercises in terms of  $err_k^{id}$  [%] by considering  
 624 sinusoidal time-varying boundary conditions, in terms of external temperature and relative  
 625 humidity.

RH	40%±10%				
Temperature	20°±5°				
Period of wet curing	1 day				
Added noise	10%				
Concrete thickness D [mm]	100			250	
Period monitored [days]	30			60	
Boundary conditions	ES	ES	EE	EE	ES
Location of discrete measurements for $h$ [mm]	/	/	50/10	125/10	125
Location of discrete measurements for $T$ [mm]	50	50/5	50	125	125
Column	A	B	C	D	E
$D_0$	1.8	2.7	1.6	5.6	3.5
$D_1$	1.2	1.3	5.4	2.4	2.7
$n$	0.8	0.7	0.6	1.0	0.4
$\kappa_{vg}^c$	1.9	1.2	7.2	4.0	3.5
$g_1$	0.9	0.6	5.4	1.5	0.8
$\gamma_c$	1.2	1.5	1.3	0.3	0.2
$\mathcal{Q}_c^{\%}$	4.6	4.0	7.0	0.9	1.0
$A_{c2}$	11.5	9.3	23.1	9.5	9.7
$\eta_c$	1.6	1.9	2.7	0.9	1.2
$k_{SH}$	2.2	2.3	0.4	0.5	0.4

626  
627

628



629

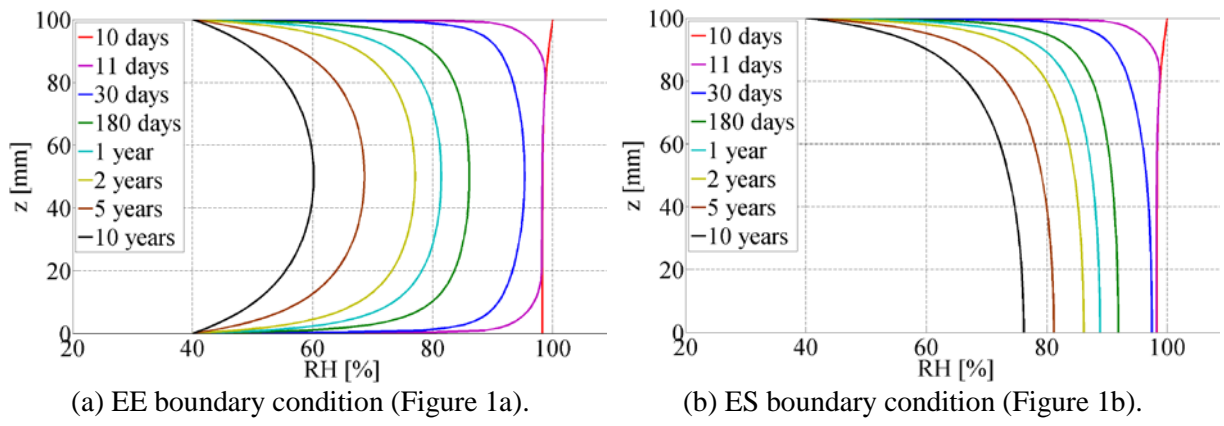
630

631

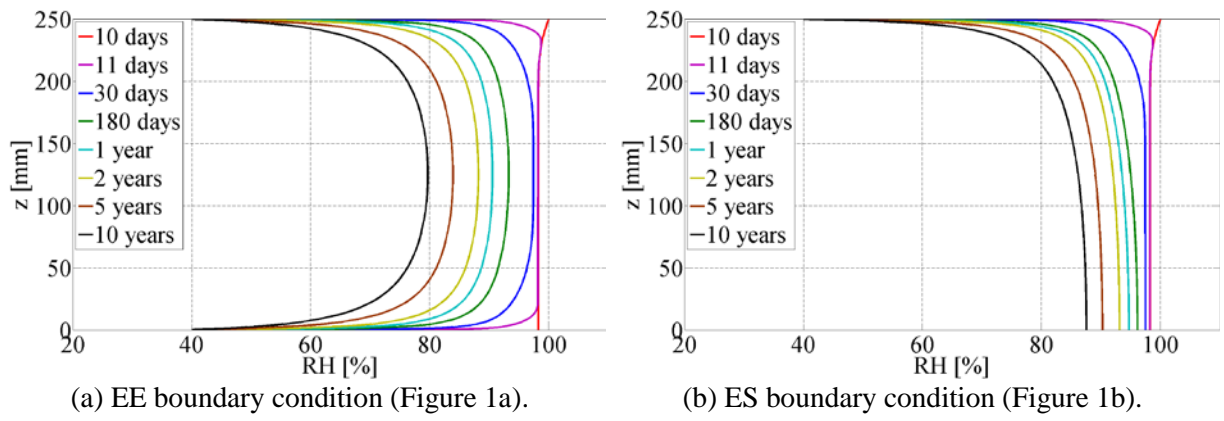
632

(a) Exposed-exposed conditions (EE)      (b) Exposed-sealed conditions (ES)

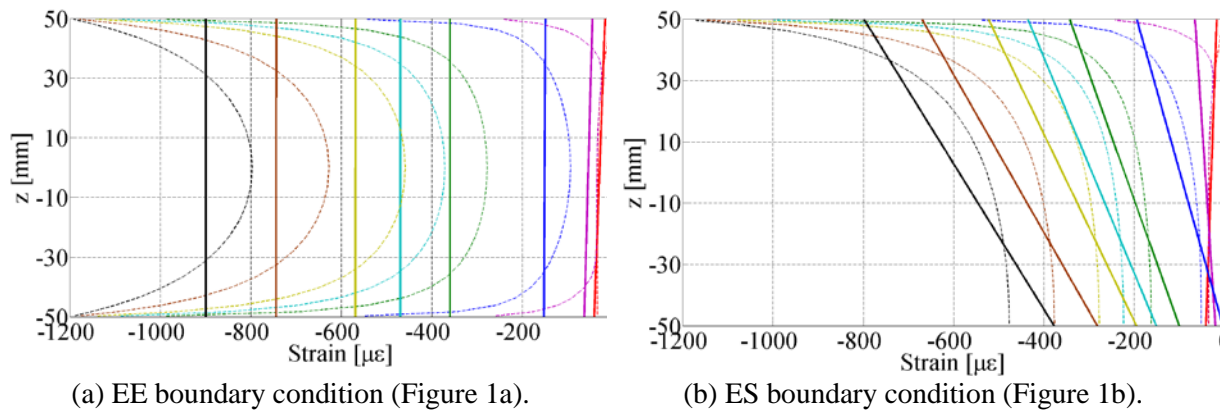
Figure 1. Boundary conditions considered for the relative humidity field.



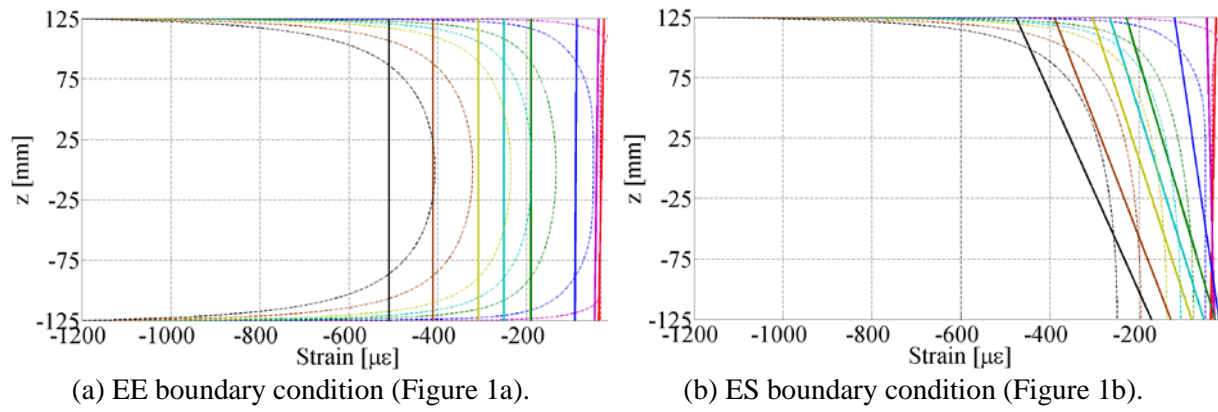
633 Figure 2. Relative humidity (RH) profiles for 10 years of simulation under different exposure  
 634 conditions for a 100 mm thick concrete component exposed to environmental RH of 40%.  
 635



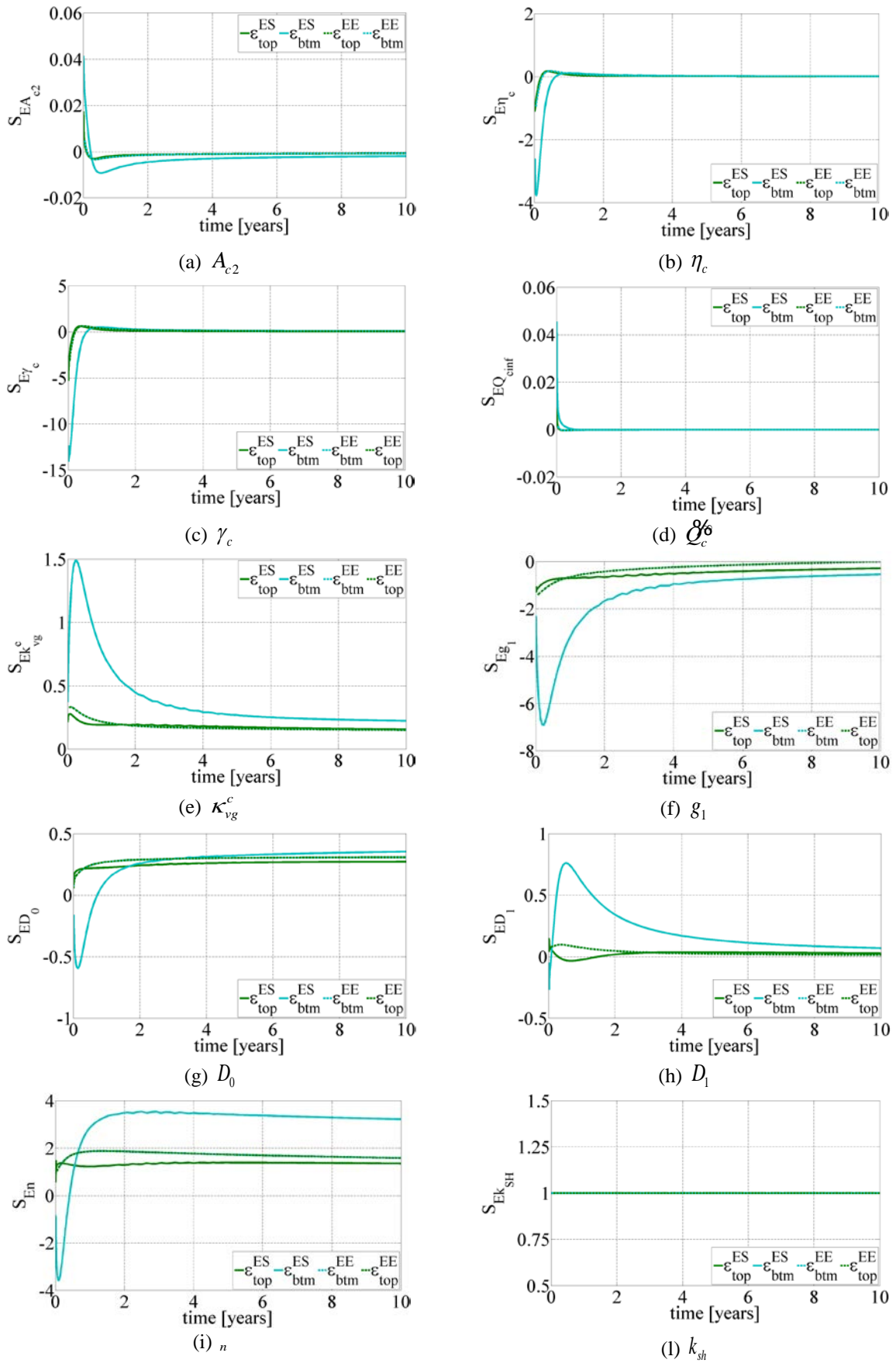
636 Figure 3. Relative humidity (RH) profiles for 10 years of simulation under different exposure  
 637 conditions for a 250 mm thick concrete component exposed to environmental RH of 40%.  
 638



639 Figure 4. Total deformations (continuous lines) and free shrinkage deformations (dotted lines)  
 640 for 10 years of simulation (at same instants in time of Figure 2) under different exposure  
 641 conditions over a 100 mm concrete thickness exposed to environmental RH of 40%.  
 642

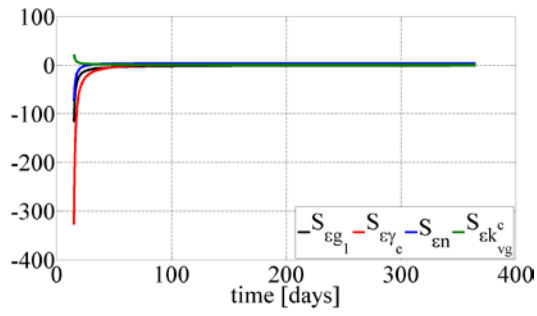


643 Figure 5. Total deformations (continuous lines) and free shrinkage deformations (dotted lines)  
 644 for 10 years of simulation (at same instants in time of Figure 3) under different exposure  
 645 conditions over a 250 mm concrete thickness exposed to environmental RH of 40%.  
 646

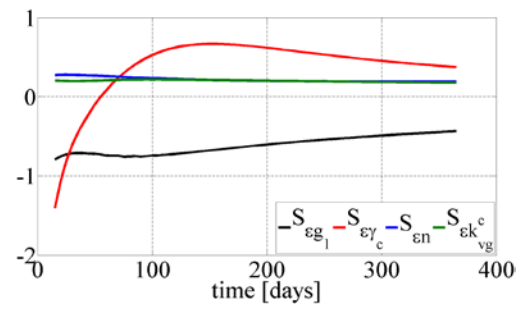


647  
 648 Figure 6. Sensitivity of deformation measurements with respect to the model parameters for a  
 649 250 mm thick concrete component and an external humidity of 40 %.

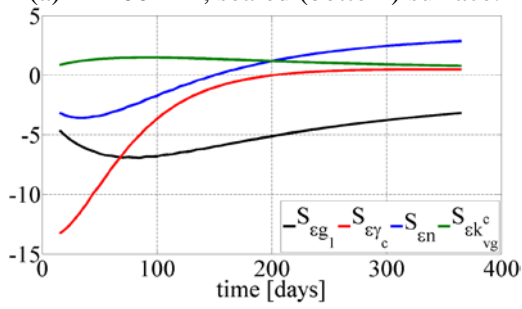




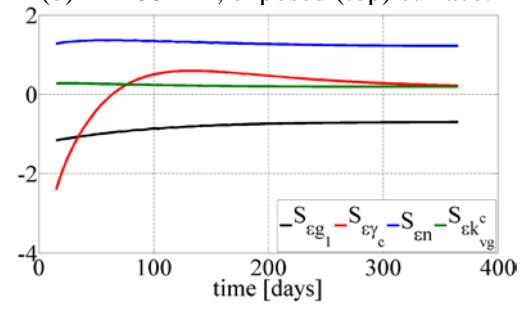
(a) D=100 mm, sealed (bottom) surface.



(b) D=100 mm, exposed (top) surface.



(c) D=250 mm, sealed (bottom) surface.



(d) D=250 mm, exposed (top) surface.

650  
 651 Figure 7. Sensitivity of deformation measurements with respect to selected model parameters  
 652 for thicknesses of 100 mm and 250 mm, and external humidity of 40%.  
 653